1990ApJ...348..333C

THE ASTROPHYSICAL JOURNAL, 348:333–340, 1990 January 1
© 1990. The American Astronomical Society. All rights reserved. Printed in U.S.A.

MOMENTUM BALANCE IN FOUR SOLAR FLARES

RICHARD C. CANFIELD
Institute for Astronomy, University of Hawaii; and University of California, San Diego
DOMINIC M. ZARRO
Applied Research Corporation at NASA/GSFC
THOMAS R. METCALF
University of California, San Diego; and Institute for Astronomy, University of Hawaii
AND
JAMES R. LEMEN
Lockheed Palo Alto Research Laboratory
Received 1988 May 6; accepted 1989 June 26

ABSTRACT

We combine *Solar Maximum Mission* soft X-ray spectra and National Solar Observatory (Sacramento Peak) Hα spectra in a study of high-speed flows during the impulsive phase of four solar flares. In all events, a blue asymmetry (indicative of upflows) was observed in the coronal Ca XIX line during the soft X-ray rise phase. In all events a red asymmetry (indicative of downflows) was observed simultaneously in chromospheric Hα. These oppositely directed flows were concurrent with impulsive hard X-ray emission. Combining the velocity data with estimates of the density based on emission measure measurements and volume estimates, we show that for the impulsive phase as a whole the total momentum of upflowing soft X-ray plasma equaled that of the downflowing Hα plasma, to within an order of magnitude, in all four events. Only the chromospheric evaporation model predicts equal total momentum in the upflowing soft X-ray–emitting and downflowing Hα–emitting material.

Subject headings: Sun: atmospheric motions — Sun: corona — Sun: flares — Sun: X-rays

I. INTRODUCTION

A key feature of the chromospheric evaporation model of solar flares is the production of simultaneous upflowing coronal and downflowing chromospheric plasmas during the impulsive phase (Kostyuk and Pikel'ner 1975; Livshits *et al.* 1981; Somov Syrovatskii, and Spektor 1981; Somov, Sermulina, , and Spektor 1982; Smith and Harmony 1982; Cheng *et al.* 1983; Fisher, Canfield, and McClymont 1985*a*; Fisher 1986). The upflowing component consists of heated soft X-ray–emitting plasma that is "evaporated" from the chromosphere (Neupert 1968; Hudson 1973; Sturrock 1973; Antonucci *et al.* 1985). The downflowing component which appeared in numerical simulations by Livshits *et al.* (1981); Somov, Syrovatskii, and Spektor (1981); Pallavicini *et al.* (1983); Nagai and Emslie 1984; MacNeice *et al.* (1984); Fisher, Canfield and McClymont (1985*a*, *b*, *c*); Karpen and DeVore (1987); Mariska, Emslie, and Li (1989)—now called the chromospheric condensation — is now understood to consist of cool, dense material, perhaps enhanced by the passage of a radiating hydrodynamic shock (Fisher, Canfield, and McClymont 1985*b*). Hα redshifts produced by the downflowing component have been observed in many flares (Svestka 1976; Tang 1983; Ichimoto and Kurokawa 1985; Canfield 1986*a*; Canfield and Metcalf 1987).

Since the chromospheric evaporation process is strictly hydrodynamic, and momentum is created in the upper preflare chromosphere, equal and oppositely directed action and reaction drive coronal plasma upward and chromospheric plasma downward. The observational verification of such conservation of momentum would be a stringent test of the chromospheric evaporation model.

We have analyzed the momentum content of observable plasmas in four solar flares for which X-ray and Hα spectral observations were obtained simultaneously using the same observing technique. Soft X-ray Ca XIX (3.176 Å) emission was observed with the X-ray Polychromator (XRP; Acton *et al.* 1980) on the *Solar Maximum Mission* (*SMM*). Hard X-rays were observed with the Hard X-ray Imaging Spectrometer (HXIS; van Beek *et al.* 1980) and the Hard X-ray Burst Spectrometer (HXRBS; Orwig, Frost, and Dennis 1980) on the *SMM*. The Hα observations were acquired with the Vacuum Tower Telescope at the National Solar Observatory (Sacramento Peak) (NSO/SP; Dunn 1969, 1971). We use these data to compute the momenta of oppositely directed flows during the impulsive phase.

In a previous paper (Zarro *et al.* 1988, hereafter Paper I), a coordinated data set enabled us to compare momentum values based on a measurement of the density of the soft X-ray–emitting flare plasma derived using the density-sensitive Ne IX triplet line ratio. Unfortunately, such line ratio observations are not available for these flares, so in the present study we use a less direct density measurement based on the observed volume and emission measure of the X-ray–emitting plasma.

II. OBSERVATIONS

The four observed flares listed in Table 1 are the only events (other than the flare described in Paper I) for which we have coordinated spectroscopic measurements of Hα and soft X-rays during the impulsive phase. They are all rather small as measured by Hα importance and *GOES* soft X-ray intensity, but in other respects they are a more diverse set. In hard X-rays they range from the dramatically varying flare 1, with a hard

© American Astronomical Society • Provided by the NASA Astrophysics Data System

1990ApJ...348..333C

TABLE 1

THE FOUR OBSERVED FLARES

Number	Date	UT	*GOES*	Hα	Location	Active Region	References
1.....	1980 May 7	14:56	C7	SB	S23 W12	2418	1, 2, 3, 4, 5
2.....	1980 Jun 23	23:12	M2	1N	S29 W08	2522	6
3.....	1980 Jun 24	15:22	M1	SB	S29 W15	2522	2, 6, 7
4.....	1980 Jun 25	15:52	M4	1B	S29 W29	2522	6, 8, 9

REFERENCES.—(1) Acton *et al.* 1982; (2) Canfield, Gunkler, and Kiplinger 1984; (3) Canfield and Gunkler 1985; (4) Simnett 1983; (5) *Solar Geophysical Data* **435**, 41 (1980), **457**, 75 (1982); (6) *Solar Geophysical Data* **436**, 42 (1980), **459**, 39 (1982); (7) Gunkler *et al.* 1984; (8) Kundu, Schmahl, and Velusamy 1982; (9) Kundu *et al.* 1985.

power-law spectrum, to the much more gradual flare 3, with an almost exponential spectrum. They also vary considerably with respect to mass ejecta; Hα movies from Big Bear Solar Observatory (BBSO) show a surge in flare 3, a filament eruption in flare 4, but no Hα eruptions of any kind in flares 1 and 2.

a) Hα Observations and Data Reduction

Hα was observed with a Fairchild 202 CCD at the reimaged focal plane of the echelle spectrograph at NSO/SP. The data consist of Hα spectra with 97.6 mÅ resolution over a 10 Å range, and spectroheliograms with 50 × 50 square pixels with 2.″55 resolution. Each pixel is sampled with a repetition period of 15 s. This description applies to flares 2, 3 and 4 (the June flares). The observations of flare 1 (the May flare) were slightly different; the spatial pixels were rectangular (2.″0 × 2.″67), and a 50 × 100 pixel spectroheliogram was generated every 25 s. Further details are given by Acton *et al.* (1982) and Gunkler *et al.* (1984).

We have examined the spectra of all spectroheliogram pixels that showed significant flare perturbation. Almost all flaring pixels show red Hα asymmetry (excess red emission), while only a few show blue asymmetry. This is consistent with Tang's (1983) study of 60 flares, in which 92% of events showed red asymmetry and 5% showed blue asymmetry. We find that pixels exhibiting blue Hα asymmetry during the impulsive phase typically had blueshifted absorption (not emission) before and early in the impulsive phase, suggesting a more direct association with filament eruptions rather than impulsive X-ray emission. We have not included blueshifted pixels in this study.

From each pixel we subtract a reference preflare profile obtained in that pixel immediately before the start of hard X-ray emission. To avoid repeated use of cumbersome terminology to distinguish such spectra, we will use the term *line profile* to denote only those data from which a reference profile has been subtracted. Figure 1 shows the temporal variation of line profiles in one of the pixels of the1980 June 23 event. The reference time was 23:09:56 UT, so the line profile at this time is flat. Only during the impulsive phase are profiles shown as the 15 s interval at which the original data were obtained.

We use extreme wing line bisectors to determine the Doppler shift velocity (see the abscissa of Fig. 1) of all redshifted pixels as a function of time. For all profiles of sufficient amplitude, bisectors are computer-drawn at the various intensity levels indicated by the horizontal lines in the figure. To ensure the ability to identify intensity-independent bisector shifts in the extreme wings, the intensity intervals are chosen to be small in the wings and large in the core. The motivation for this choice of intensity levels is the demonstration by Ichimoto and Kurokawa (1985) that strongly redshifted impulsive phase Hα profiles are symmetric about a shifted centroid in the profile wings. This is equivalent to a wing bisector shift that is independent of intensity (see Fig. 1 profiles at 23:12:11 and several other times). In those spectra for which this is not true (e.g., 23:11:26 UT), we adopt the maximum observed shift. Theoretical work on Hα line formation (Canfield and Gayley 1987) in downflowing chromospheric condensations (Fisher, Canfield, and McClymont 1985*b*) shows that broad redshifted Hα emission comes from the moving condensation, lending credence to the Ichimoto and Kurokawa approach.

The Hα parameters of the analysis below are given in Table 2. The maximum observed value of the downflow velocity v_d and the characteristic time τ for it to decay to half its maximum value are averages of these quantities for all pixels that show significant redshifts. Since only a fraction of the spectra fail to show intensity-independent wing bisector shifts, we adopt the average as a proper approximation, rather than a lower limit. The chromospheric downflow area S_c is taken to be the sum of the areas of all such pixels; possible effects of under resolution will be discussed below. For all flares, we identify footpoints of opposite magnetic polarity on the basis of coaligned Hα spectroheliograms and magnetograms from National Solar Observatory (Kitt Peak) (KPNO). Assuming that the footpoints are connected by a semicircular coronal arch, we derive a loop half-length $L = \pi D/4$, where D is the footpoint separation. Assuming that the loop cross sectional area is $A = S_c/2$, we compute a characteristic loop volume $V = 2AL$.

b) X-Ray Observations and Data Reduction

The XRP instrument consists of two Bragg spectrometers: a Flat Crystal Spectrometer (FCS) and a Bent Crystal Spectrometer (BCS). The FCS has a 14″ collimated field of view which, prior to the impulsive phase of each flare, was rastered over a 4′ × 4′ field of view in 15″ steps. These rasters produced X-ray images in the O VIII (18.97 Å) and Mg XI (9.17 Å) lines, which are formed at temperatures in the range 2×10^6 K $< T < 7 \times 10^6$ K. From the ratio of the fluxes in these two optically thin lines, we derive the characteristic coronal temperature of the preflare active region. We estimate an error of $\pm 1 \times 10^6$ K in the preflare temperature.

The BCS has a 6′ collimated field of view which observes the Ca XVIII–XIX (3.17–3.26 Å) line complex with 3 s temporal resolution and 0.9 mÅ spectral resolution. Figure 2 illustrates the Ca XIX resonance line profile in each flare, derived by summing individual spectra during the rise phase of soft X-rays (given below for each flare). It has been shown by Antonucci, Gabriel, and Dennis (1984) that Ca XIX blueshifts decay rapidly early in the impulsive phase, stabilizing late in the decay phase. Accordingly, we have calibrated the wavelength

© American Astronomical Society • Provided by the NASA Astrophysics Data System

1990ApJ...348..333C

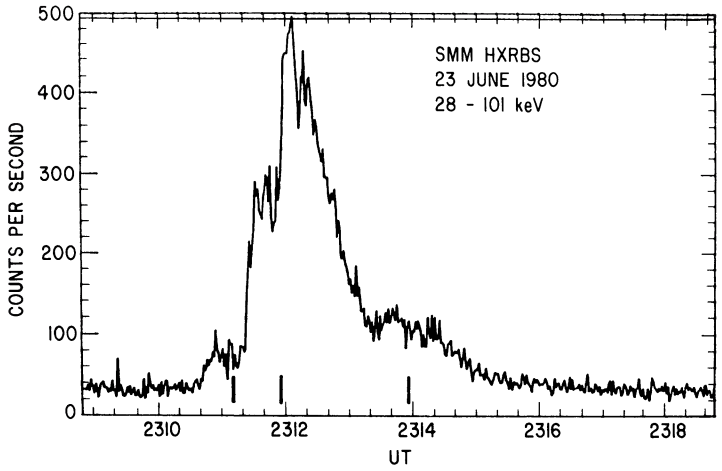

FIG. 1*a*

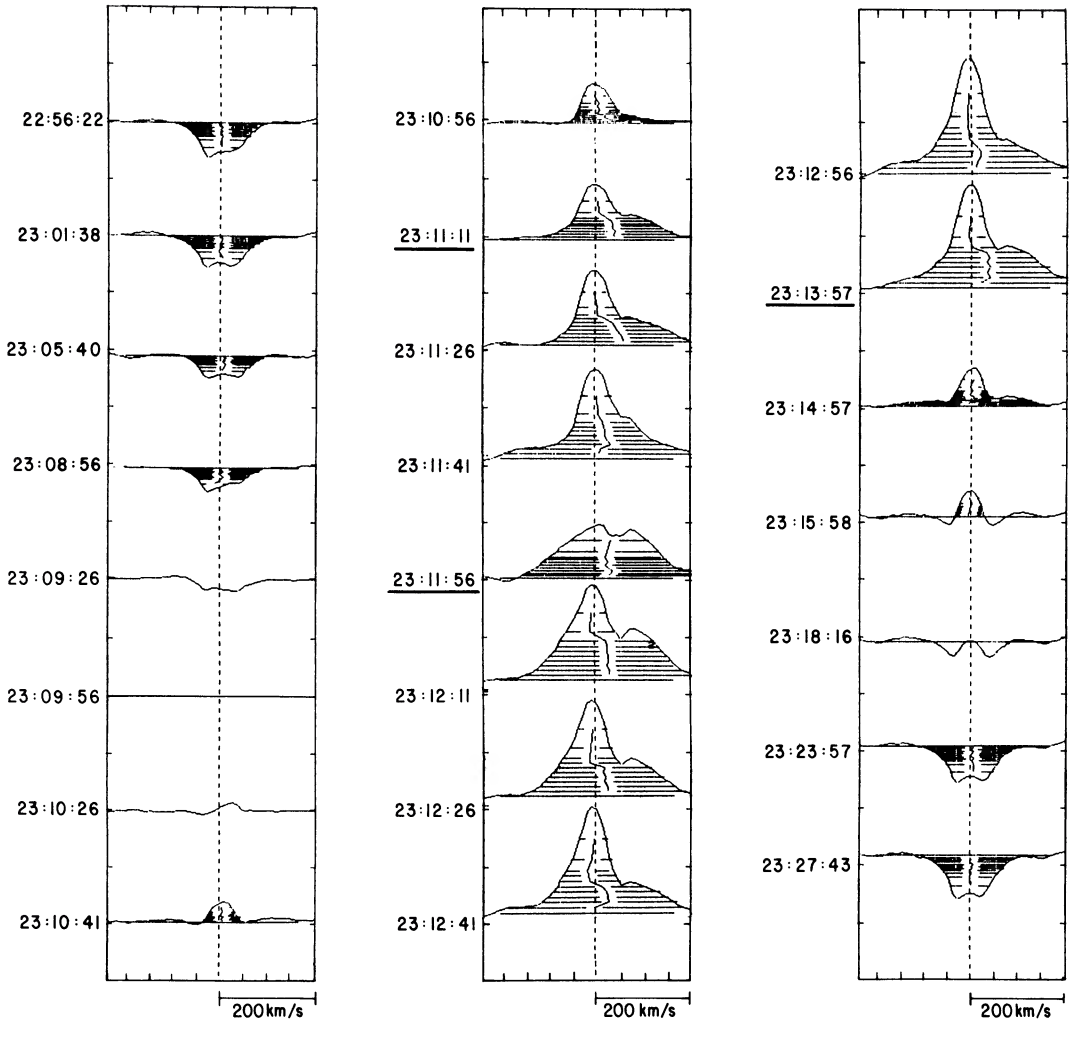

FIG. 1*b*

FIG. 1.—Hα and hard X-ray observations of the flare of 1980 June 23. *Upper panel:* the hard X-ray count rate observed by the *SMM* Hard X-ray Burst Spectrometer. *Lower panel*: the Hα line profiles of a single pixel observed at SPO, with bisectors drawn at the intensity levels indicated by the horizontal striations centered within the most intense emission.

© American Astronomical Society • Provided by the NASA Astrophysics Data System

1990ApJ...348..333C

TABLE 2

PARAMETERS OF THE MOMENTUM ANALYSIS

Parameter	1980 May 7	1980 Jun 23	1980 Jun 24	1980 Jun 25
		Hα		
v_d(km s^{-1})	41 ± 8	42 ± 8	37 ± 12	24 ± 12
τ(s)	36 ± 16	30 ± 12	30 ± 12	28 ± 15
S_c(cm^2)	1.1×10^{17}	3.5×10^{17}	4.5×10^{17}	5.2×10^{17}
L(cm)	5.7×10^{8}	7.3×10^{8}	6.5×10^{8}	1.0×10^{9}
		Soft X-Ray		
V(cm^3)	6.3×10^{25}	2.6×10^{26}	2.9×10^{26}	5.2×10^{26}
EM(cm^{-3})	$5.7 \pm 0.8 \times 10^{48}$	$1.7 \pm 0.5 \times 10^{48}$	$6.6 \pm 1.0 \times 10^{48}$	$2.8 \pm 0.5 \times 10^{49}$
T_0(K)	3.0×10^{6}	3.4×10^{6}	3.8×10^{6}	3.4×10^{6}
v_u(km s^{-1})	264 ± 50	323 ± 40	336 ± 60	344 ± 40
		Results		
P_c(dyn cm^{-2})	20.	23.	37.	17.
n_c(cm^{-3})	1.8×10^{13}	2.1×10^{13}	3.4×10^{13}	1.5×10^{13}
p_u(g cm s^{-1})	1.3×10^{21}	1.8×10^{21}	3.8×10^{21}	11.1×10^{21}
p_d(g cm s^{-1})	3.1×10^{21}	$10. \times 10^{21}$	16×10^{21}	3.3×10^{21}

scale for each spectrum in Figure 2 by fitting the lines comprising the Ca XVII–XIX complex and setting their centroids to their known rest wavelengths. Theoretical models (e.g., Emslie and Alexander 1987) indicate that only a small error arises in this process.

The impulsive phase profiles exhibit the characteristic blue symmetry indicative of upflows attributed to chromospheric evaporation (Antonucci *et al.* 1985). We parameterize the asymmetry by least-squares fitting a double Voigt function to each profile. The fitted functions are superposed as smooth solid lines on the Ca XIX spectra; the dashed lines represent the weaker blueshifted emission in the Ca XIX wing. We derive a characteristic upflow velocity v_u from the separation of the two components; clearly the weakness of the blueshifted component does not allow a multiparameter approach. Note that the fits do not extend into the red wing of the Ca XIX resonance lines in order to avoid the effects of the $n \geq 3$ satellites in this region. Further details of the fitting procedure are given in Fludra *et al.* (1989).

From the strength of the Ca XIX resonance line at flare maximum and the electron temperature derived from the Ca XVIII to Ca XIX line ratio (Bely-Dubau *et al.* 1982), we

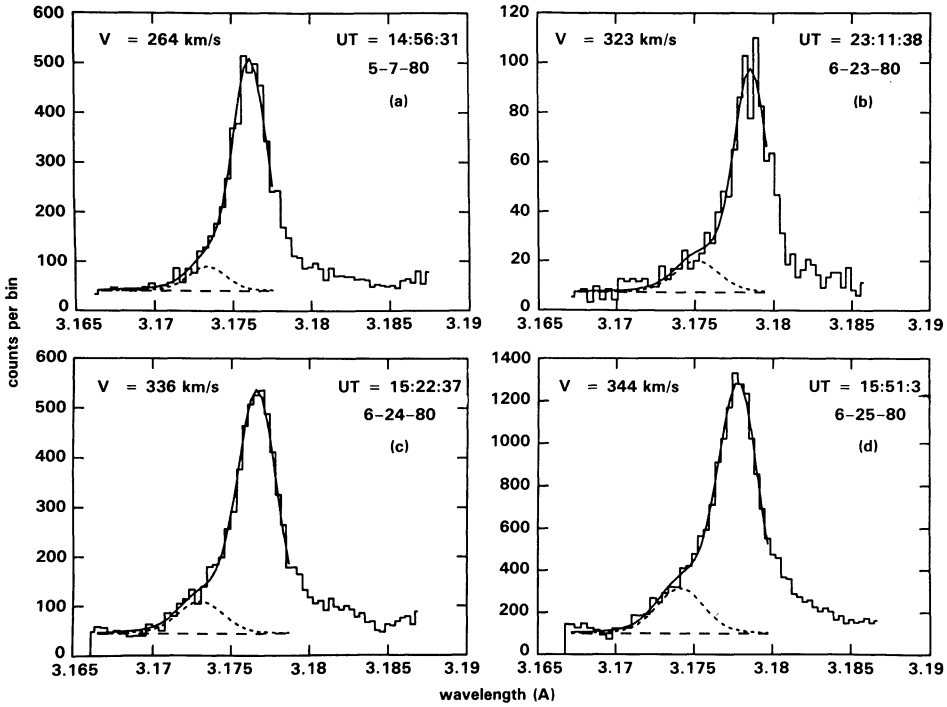

FIG. 2.—The BCS Ca XIX profiles integrated over the soft X-ray rise phase of each of the four flares. The indicated time denotes the middle of the rise phase in each event. The smooth line represents a two-component Voigt function model fit to the profile. The dotted line shows the secondary component at the indicated blueshift velocity.

© American Astronomical Society • Provided by the NASA Astrophysics Data System

1990ApJ...348..333C

compute the emission measure ($EM = \int n_e^2 dV$) of flare plasma. Given the loop volume V and mass conservation, the total number of evaporated atoms in the coronal soft X-ray source is approximately $(EM\ V)^{1/2}$. The parameters of the soft X-ray analysis are listed in Table 2. The quoted uncertainties for the upflow velocity and emission measure are derived from the formal errors of the Ca XIX profile fitting procedure.

c) *The Flare of 1980 May 7*

This flare was analyzed by Acton *et al.* (1982) and Canfield and Gunkler (1985). The lack of observed Hα ejecta in this event places it in the category of a compact flare (Pallavicini, Serio, and Vaiana 1977). On the basis of coaligned magnetograms, SPO Hα spectroheliograms, and HXIS X-ray images, Acton *et al.* (1982) identified a loop structure with two well-defined footpoints separated by 10″, corresponding to a loop half-length $L = 5.7 \times 10^8$ cm. The Hα red asymmetry was confined to four pixels, corresponding to an area of $S_c = 1.1 \times 10^7$ cm^2. Combining these two quantities, we compute a loop volume of $V = 6.3 \times 10^{25}$ cm^3, which is consistent with that derived by Acton *et al.* (1982). The average value of the maximum Doppler shift velocity for these four Hα pixels is $v_d = 41 \pm 8$ km s^{-1}, and the characteristic decay time $\tau = 36 \pm 16$ s. The preflare Mg XI/O VIII line ratios imply a preflare coronal temperature of 3.0×10^6 K.

The flare impulsive phase consisted of two periods of hard X-ray emission extending from 14:56:03 to 14:56:12 UT, and 14:56:24 to 14:56:47 UT. Soft X-ray Ca XIX emission commenced at 14:56 UT and peaked at 14:57:30 UT. A two component fit to the Ca XIX profile integrated over this period (Fig. 2*a*) gives a characteristic upflow velocity of 264 ± 50 km s^{-1}. The peak emission measure derived from the Ca XIX intensity is $5.7 \pm 0.8 \times 10^{48}$ cm^{-3}.

d) *The Flare of 1980 June 23*

Since this event has not been studied previously, it is necessary to establish its morphology. We have coaligned SPO flare-excess Hα spectroheliograms averaged during the period 23:12:06 UT to 23:12:18 UT with a KPNO magnetogram obtained at 13:49 UT. Because almost 10 hr elapsed between the KPNO magnetogram and the flare, it would not be surprising to find misalignment of several arcsec (1–2 SPO pixels). Figures 3*a* and 3*b* (Plates 1–2) display the corresponding Hα red wing and blue wing images derived by averaging 1 Å regions centered ±2 Å from line center. Based on a comparison with the magnetogram, we identify the NW and SE regions in the red wing image as the opposite polarity footpoints of a coronal loop. The loop does not precisely span the line of polarity reversal, which we ascribe to poor coalignment owing to the 10 hr time difference of the SPO and KPNO data. The separation of these two regions implies a loop half-length of 7.3×10^8 cm. Figure 1 shows the temporal variation of Hα profiles in one of the pixels in the NW region. From the total number of pixels with significant Hα redshifts, we determine a downward-moving chromospheric area of 3.5×10^{17} cm^2. These values imply a loop volume of 2.6×10^{26} cm^3. From the spectra of the pixels within the downflowing region, we derive an average value of the peak redshift of 42 ± 8 km s^{-1}, and a corresponding decay time of 30 ± 12 s.

The blue wing image shows two main features. The first coincides with the red wing NW region. The second and larger feature has no counterpart in the red wing image, but coincides with an erupting filament with higher resolution in BBSO Hα movies. The SPO Hα spectra at this location reveal a blue-shifted feature that changes from absorption to emission during the impulsive phase.

The preflare temperature of the active region determined from FCS line ratios was 3.4×10^6 K. This value is uncertain due to the fact that the preflare FCS image of the active region did not include the flaring portion observed by SPO in Hα. We shall henceforth assume that this temperature is also characteristic of the preflare value at the site of Hα emission.

The event was relatively impulsive in hard X-rays, as shown in the upper panel of Figure 1. Hard X-rays commenced at 23:10:30 UT, peaked at 23:12:08 UT, and ended at 23:16 UT. Soft X-ray emission showed a smooth rise commencing at 23:10:30 UT and peaking at 23:13:10 UT. From the Ca XIX resonance line profile (Fig. 2*b*) integrated over this period, we deduce an upflow velocity of 323 ± 40 km s^{-1}. From the strength of the Ca XIX resonance line at soft X-ray maximum, we compute an emission measure of $1.7 \pm 0.5 \times 10^{48}$ cm^{-3}. This value is the lowest of the four flares.

e) *The Flare of 1980 June 24*

Using co-aligned magnetograms, SPO Hα spectroheliograms, and HXIS images of this event, Gunkler *et al.* (1984) inferred the existence of two arcades of coronal loops, which they denoted as N-W and E-C. They also observed an Hα surge which began before the impulsive phase, and was not in the N-W loop system. Redshifted Hα spectra indicate that downflow motions are confined to the N-W system, which has a characteristic loop half-length of 6.5×10^8 cm. The spectroheliograms show 13 redshifted pixels associated with this system, corresponding to an area of 4.5×10^{17} cm^2. Comparison with BBSO Hα images suggests that there may be a small number of redshifted pixels in the N-W region outside the SPO field of view. The neglect of these additional pixels introduces a small uncertainty in the downflow area. Combining these two geometric quantities, we compute a loop volume of 2.9×10^{26} cm^3. Averaging over the observed redshifted pixels, we derive a peak downflow velocity of 37 ± 12 km s^{-1} with a characteristic decay time of 30 ± 12 s.

From the FCS Mg XI/O VIII soft X-ray line ratios, we compute a preflare coronal temperature of 3.8×10^6 K for this event. Hard X-ray emission began at 15:21:50 UT, peaked at 15:22:50 UT, and decreased smoothly to background with a characteristic time scale of about 1 minute. Analysis of the Ca XIX profile (Fig. 2*c*) integrated during the soft X-ray rise phase (15:20:45–15:24:10 UT) indicates an upflow velocity of 336 ± 60 km s^{-1}. At the time of peak Ca XIX emission, we estimate a total emission measure of $6.6 \pm 1.0 \times 10^{48}$ cm^{-3}.

f) *The Flare of 1980 June 25*

The morphology of this flare is well known based on previous studies by Kundu, Schmahl, and Velusamy (1982) and Kundu *et al.* (1985). All redshifted pixels are located in regions 1 and 2 (using the notation of Kundu, Schmahl, and Velusamy 1982), which lie on opposite sides of the magnetic neutral line. A total of 15 redshifted pixels implies a downflow area of 5.2×10^{17} cm^2. The mean separation of the opposite polarity regions yields a loop half-length of 1.0×10^9 cm. Hence, the coronal volume is 5.2×10^{26} cm^3. From spectra of pixels

© American Astronomical Society • Provided by the NASA Astrophysics Data System

1990ApJ...348..333C

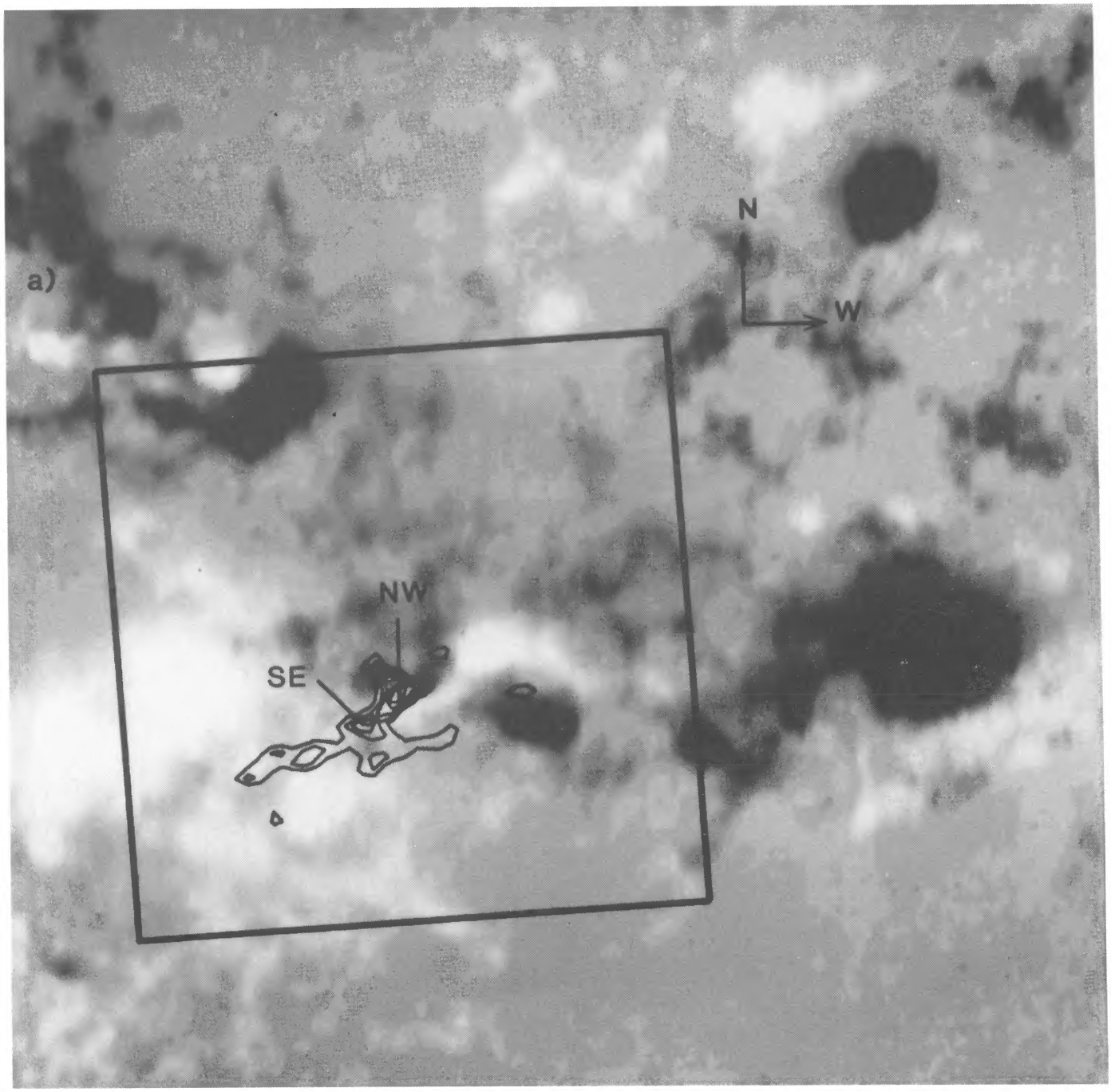

FIG. 3a

FIG. 3.—KPNO line-of-site magnetogram of active region AR 2522 associated with the flare of 1980 June 23. Positive polarity regions appear white; negative appear black. The square box denotes the SPO 2'.1 × 2'.1 field of view. The superposed contours in Fig. 3*a* indicate the intensity (preflare subtracted) in the Hα red wing, derived by averaging over a 1 Å band centered 2 Å from line center during the impulsive phase. The regions marked NW and SE denote opposite polarity footprints of the soft X-ray emitting coronal loop. The superposed contours in Fig. 3*b* show the corresponding intensity at −2 Å from line center, in the Hα blue wing, during the impulsive phase. The blue wing image shows two main features. The first coincides with the red wing NW region. The second and larger feature has no counterpart in the red wing image, but coincides with an erupting filament seen in Hα.

© American Astronomical Society • Provided by the NASA Astrophysics Data System

1990ApJ...348..333C

PLATE 2

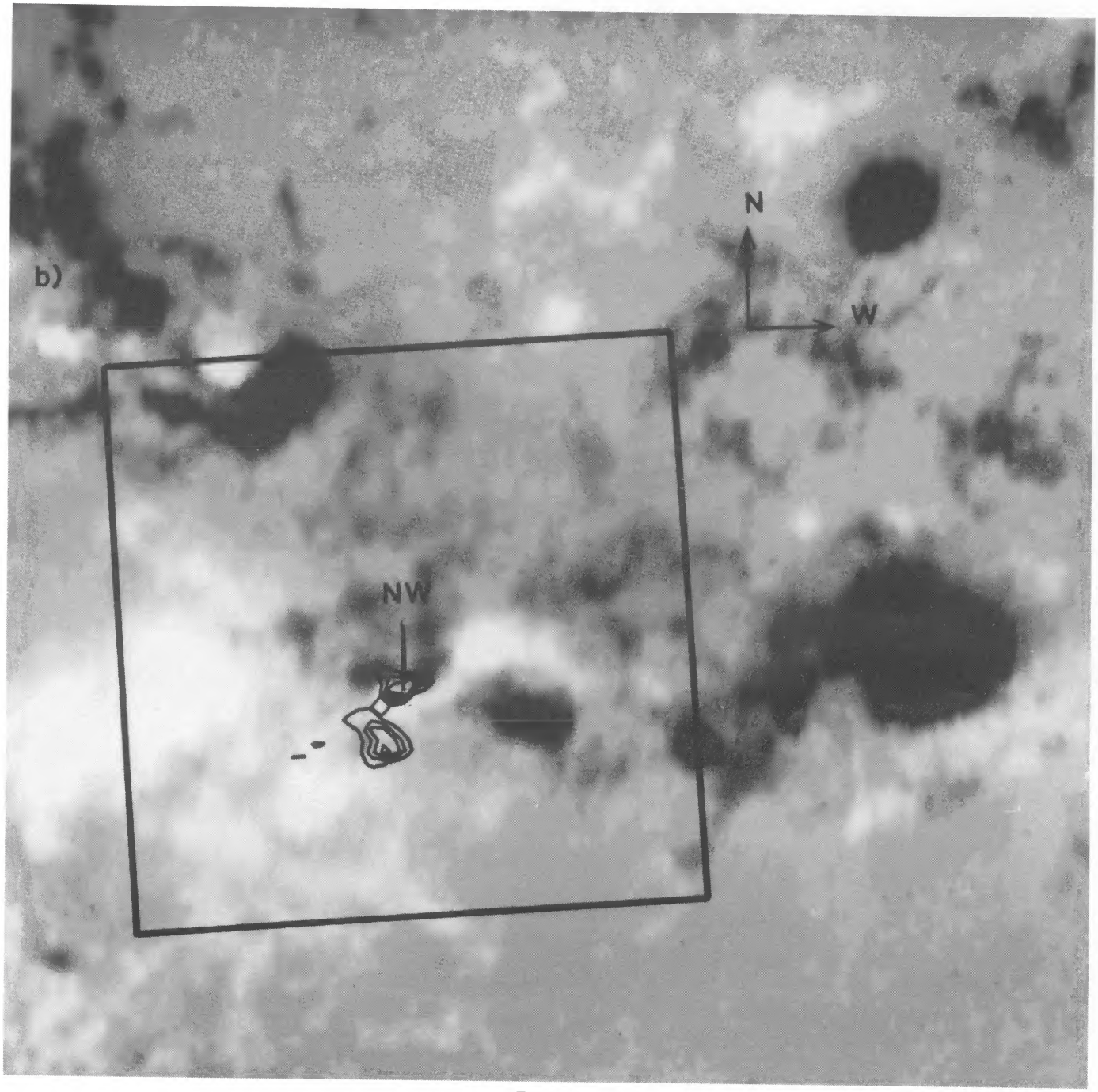

FIG. 3*b*

CANFIELD, ZARRO, METCALF, AND LEMON (*see* **348**, 337)

© American Astronomical Society • Provided by the NASA Astrophysics Data System

1990ApJ...348..333C

within the downflowing region, we derive an average value of the peak redshift of 24 ± 12 km s^{-1} and a corresponding decay time of 28 ± 15 s. A preflare temperature could not be derived for this event since FCS line ratio observations were not obtained. Consequently, we adopt a value of 3.4×10^6 K, which is the average of preflare temperatures derived from the preceding events.

Hard X-ray emission began at 15:50:00 UT, peaked at 15:52:00 UT, and ended at 15:58 UT. From the Ca XIX resonance line profile (Fig. 2*d*) integrated over the rise phase (15:50:00–15:52:05 UT), we derive an upflow velocity of 344 ± 40 km s^{-1}. At soft X-ray maximum, we compute a soft X-ray emission measure of $2.8 \pm 0.5 \times 10^{49}$ cm^{-3}.

III. AN APPROXIMATE MOMENTUM ANALYSIS

We follow the analysis of Ichimoto and Kurokawa (1985) and Paper I, in which one determines the total momentum that the flowing material would have if it were not brought to a stop by the confining loop, and in which one integrates over the impulsive phase of the flare. Throughout this work we will define the term total momentum to mean this integrated quantity, in contrast to the instantaneous momentum.

The total impulsive phase momentum p_u of the coronal plasma upflowing at velocity v_u to contribute to the total number of coronal ions given by (EM V)$^{1/2}$ at the end of the rise phase of soft X-rays is

$$p_u = \mu m_{\rm H} v_u \sqrt{\rm EM\ V}\ , \qquad (1)$$

where the mean atomic mass μ is taken to be 1.56, and $m_{\rm H}$ is the mass of atomic hydrogen.

This approach assumes that the momentum of the upflowing material can satisfactorily be modeled by a suitably defined constant velocity and density. Using the chromospheric evaporation model of Fisher (1986), it is easily shown that this approach leads to an error of only $2^{1/2}$—quite adequate for our order-of-magnitude analysis. Further, we use the observed Ca XIX blueshift velocities for the values of v_u; observed velocities for ions of different temperatures deviate from that of Ca XIX by less than a factor of 2 (cf. Zarro, Slater, and Freeland for Mg XI and Antonucci and Dodero 1986 and Antonucci 1989 for Fe XXV). A potentially greater error may arise because we are obliged to use (EM V)$^{1/2}$ to estimate the total number of atoms, and the results is therefore sensitive to volume uncertainties and density variations (discussed below).

We identify the matter that emits redshifted Hα with the chromospheric condensation phenomenon discussed by Fisher, Canfield, and McClymont (1985*b*) and other authors (see § I). Moving at supersonic velocity v_d into the chromosphere, the condensation accretes material at a rate (per unit area) $m_{\rm H} n_c v_d$, where n_c is the preflare (upstream) chromospheric density. After a characteristic time τ (see § II*a*) the total momentum of the downflowing material is

$$p_d = \mu m_{\rm H} n_c S_c v_d^2 \tau\ . \qquad (2)$$

The preflare chromospheric density n_c is obtained by a scaling-law approach. Substituting the observed preflare coronal temperature and loop half-length into the conduction-dominated loop scaling law of Craig, McClymont, and Underwood (1978), we derive a preflare coronal pressure P_c. Assuming hydrostatic equilibrium (and neglecting the small gravitational contribution term), the preflare pressure at the top of the chromosphere equals that of the corona. The values of P_c and n_c are listed in Table 2, where we have assumed a preflare chromospheric temperature of 8000 K.

The dominant source of error in the upflow momentum is the estimate of the coronal volume, which depends on the assumed geometry. The assumption of a uniform semicircular arch is certainly simplistic, although there is no more appropriate assumption. Volumes derived using different geometrical forms vary typically by a factor of 2 (cf. Acton *et al.* 1982; Gunkler *et al.* 1984). Formal errors in the upflow velocity and coronal emission measure are about 20%. Hence, the computed upflow momentum is uncertain by at least a factor of 2.

The preflare chromospheric density accounts for an uncertainty of approximately a factor of 2 in the downflow momentum. The strong temperature dependence of the loop scaling law magnifies small uncertainties in the preflare temperature to larger errors in the coronal pressure and, hence, chromospheric density. Another factor of 2 uncertainty arises from the velocity squared term; the formal error in the velocity ranges from 20% to 50%. Of course, the extent to which each pixel is filled by moving material is not known. Hence, the computed downflow momentum is uncertain by at least a factor of 4, and is an upper limit, because S_c is an upper limit.

Does the ratio of upflow to downflow momenta depend sensitively on departures from a uniform distribution of plasma? Since magnetic pressure dominates gas pressure in both the chromosphere and the corona, it is reasonable to adopt the same filling factor and cross sectional area in both regions. Defining f to be the fraction of V that is filled by X-ray–emitting plasma, $p_u \propto V^{1/2} \propto f^{1/2}$ and $p_d \propto S_c \propto f^{2/3}$, so their ratio scales as $f^{1/6}$.

Substituting the values of the chromospheric and coronal parameters into the above equations, we derive the momentum values given in Table 2. For the first three flares $p_u < p_d$ (by factors up to ≈ 5) and for the fourth flare $p_u > p_d$ (by a factor of ≈ 3). Given the small number of events, a statistical approach is not appropriate. In view of the uncertainties in the data and the approximate nature of the analysis, the upflow and downflow momenta can be considered equal, to order of magnitude.

IV. DISCUSSION

The momentum content of soft X-ray upflows and Hα downflows during the impulsive phase of these four flares has been found equal to its order-of-magnitude measurement and analysis uncertainty. It is noteworthy that this result has been found in flares that show clear evidence of ejection of Hα material in the form of surges and filament eruptions, as well as flares that show no such evidence.

The result has important implications for the debate over the physical interpretation of observed impulsive-phase X-ray blueshifts (Doschek *et al.* 1986; Canfield 1986*b*). Various physical scenarios have been proposed that can explain the soft X-ray blueshifts, but fail to predict Hα redshifts that carry equal total momentum.

In the *magnetohydrodynamic* scenario (Karpen, Doschek, and Seely 1986), the sudden heating of twisted flux tubes produces gas expulsion due to imperfect magnetic field confinement. The consequent plasma motions are directed away from the solar surface toward regions of weaker magnetic field strength. Hence, both the soft X-ray and Hα plasmas are ejected outward—contrary to our observations showing that they are oppositely directed.

© American Astronomical Society • Provided by the NASA Astrophysics Data System

1990ApJ...348..333C

In the *reconnecting loop* scenario (Doschek *et al.* 1986), an emerging dense flux tube collides with an overlying low density loop. Following reconnection, the pressure difference between the two loops drives an upflow of heated plasma into the overlying loop, producing a soft X-ray blueshift. Although Doschek *et al.* (1986) did not discuss the issue, it can be shown that the high coronal pressures created impulsively in the low-lying loop will drive very fast downflows (≈ 200 km s^{-1}) in the Hα-emitting chromosphere at the footpoints. Such large velocities of Hα-emitting material are not observed. Moreover, in this model most of the X-rays are hypothesized to come from the low-lying loop, in which material is stationary; the implied dominance of the momentum budget by downflowing material contradicts our observations of oppositely directed flows that carry approximately equal amounts of momentum.

In the *current filamentation* model of electron beams (Winglee, Pritchett, and Dulk 1988), coronal ions are heated in the direction perpendicular to the magnetic field and tend to flow upward (due to the mirror force) if coronal magnetic fields converge near their footpoints. The reaction to the mirror force is imparted to the matter to which the field lines are rooted, and this line tying occurs far below the visible surface (McClymont 1990). This model thus fails to predict oppositely directed chromospheric and coronal flows.

In the *untwisting flux tube* model (Uchida and Shibata 1988), a flux tube emerging from the gas pressure dominated photosphere unwinds when gas pressure forces can no longer keep it twisted. As it unwinds, the tube ejects entrained plasma upward, heating it to soft X-ray temperatures. In this model, the dominant forces are hydromagnetic, not hydrodynamic, so the dominant motion is upward. Again, the reaction is transferred by the magnetic field to great depths at which line tying is achieved.

Finally, Batchelor (1986) suggested that the observed soft X-ray blueshifts can be attributed to material in or surrounding an erupting filament in at least one well-observed flare. This suggestion makes no prediction regarding the existence of a downflowing component. The fact that we find momentum balance between observed upflows and downflows in events both with and without filaments (neglecting blueshifted Hα material) suggests that this mechanism is not dominant in the production of soft X-ray blueshifts.

In the *chromospheric evaporation* model (e.g., Fisher, Canfield, and McClymont 1985*a*), the sudden creation of a high-pressure region at the footpoint of a coronal loop produces upflowing hot (coronal) plasma and downflowing cool (chromospheric) plasma. This simple hydrodynamic model predicts the observed equal and opposite momenta of the upflowing coronal and downflowing chromospheric plasmas during the flare impulsive phase.

One would need several improvements over the present observations to justify a more rigorous comparison of theory and observation. Coordinated Hα and X-ray spectra are presently available for only five flares, which is an insufficiently large number to justify a statistical comparison. Future improvements in spectroscopy may enable a comparison of *instantaneous* momentum values early in the impulsive phase. One would like to be able to study the momentum content of spatially and temporally resolved *components* of flares, to discriminate more compellingly between energy transport mechanisms and more global hydromagnetic flare models. At this time the main observational stumbling blocks are inadequate temporal and spatial resolution of both thermal X-rays and chromospheric Hα.

We thank George Fisher and Sandy McClymont for helpful discussions. The work performed at the Goddard Space Flight Center was supported by NASA contract NAS5-28713 and the Lockheed Independent Research Program. The work performed at the University of Hawaii was supported by National Science Foundation grant AST-8615358 and AST-8900716.

REFERENCES

Acton, L. W., *et al.* 1980, *Solar Phys.*, **65**, 53.
Acton, L. W., *et al.* 1982, *Ap. J.*, **263**, 409.
Antonucci, E. 1989, in *IAU Colloquium 104, Solar and Stellar Flares*, ed. B. Haisch and M. Rodonò, in press.
Antonucci, E., Dennis, B. R., Gabriel, A. H., and Simnett, G. M. 1985, *Solar Phys.*, **96**, 129.
Antonucci, E., and Dodero, M. A. 1986, in *The Lower Atmosphere in Solar Flares*, ed. D. Neidig (Sunspot, N.M.: National Solar Observatory), p. 363.
Antonucci, E., Gabriel, A. H., and Dennis, B. R. 1984, *Ap. J.*, **287**, 917.
Batchelor, D. A. 1986, in *Adv. Space Res.*, Vol. **6**, No. 6, p. 159.
Bely-Dubau, F., *et al.* 1982, *M.N.R.A.S.*, **201**, 1155.
Canfield, R. C. 1986*a*, in *The Lower Atmosphere in Solar Flares*, ed. D. Neidig (Sunspot, N.M.: National Solar Observatory), p. 10.
———. 1986*b*, in *Adv. Space Res.*, Vol. **6**, No. 6, p. 167.
Canfield, R. C., and Gayley, K. G. 1987, *Ap. J.*, **322**, 999.
Canfield, R. C., and Gunkler, T. A. 1985, *Ap. J.*, **288**, 353.
Canfield, R. C., Gunkler, T. A., and Kiplinger, A. L. 1984, *Adv. Space Res.*, Vol. **4**, No. 7, p. 225.
Canfield, R. C., and Metcalf, T. R. 1987, *Ap. J.*, **321**, 586.
Cheng, C.-C., Oran, E. S., Doschek, G. A., Boris, J. P., and Mariska, J. T. 1983, *Ap. J.*, **265**, 1090.
Craig, I. J. D., McClymont, A. N., and Underwood, J. H. 1978, *Astr. Ap.*, **70**, 1.
Doschek, G. A., *et al.* 1986, in *Proc. SMM Workshop, Energetic Phenomena on the Sun*, ed. M. R. Kundu and B. Woodgate (NASA CP-2439), p. 4-1.
Dunn, R. B. 1969, *Sky and Tel.*, **38**, 1.
———. 1971, in *The Menzel Symposium on Solar Physics, Atomic Spectra, and Gaseous Nebulae*, ed. K. B. Gebbie (NBS Spec. Pub. 353) (Washington: US Government Printing Office), p. 71.
Emslie, A. G., and Alexander, D. 1987, *Solar Phys.*, **110**, 295.
Fisher, G. H. 1986, in *Lecture Notes in Physics*, Vol. **255**, *Radiation Hydrodynamics in Stars and Compact Objects*, ed. D. Mihalas and K.-H. A. Winkler (Berlin: Springer-Verlag), p. 53.
Fisher, G. H., Canfield, R. C., and McClymont, A. N. 1985*a*, *Ap. J.*, **289**, 414.
Fisher, G. H., Canfield, R. C., and McClymont, A. N. 1985*b*, *Ap. J.*, **289**, 434.
———. 1985*c*, *Ap. J.*, **289**, 425.
Fludra, A., Lemen, J., Jakimiec, J., Bentley, R. D., and Sylwester, J. 1989, *Ap. J.*, **344**, 991.
Gunkler, T. A., Acton, L. W., Canfield, R. C., and Kiplinger, A. L. 1984, *Ap. J.*, **285**, 835.
Hudson, H. S. 1973, in *Symposium on High Energy Phenomena on the Sun*, ed. R. Ramaty and R. G. Stone (Goddard SFC Rept. X-693-73-193), p. 207.
Ichimoto, K., and Kurokawa, H. 1985, *Solar Phys.*, **93**, 105.
Karpen, J. T., and Devore, R. C. 1987, *Ap. J.*, **320**, 904.
Karpen, J. T., Doschek, G. A., and Seely, J. F. 1986, *Ap. J.*, **306**, 327.
Kostyuk, N. D., and Pikel'ner, S. R. 1975, *Sov. Astr.*, **18**, 590.
Kundu, M. R., Gaizauskas, V., Woodgate, B. E., Schmahl, E. J., Shine, R., and Jones, H. P. 1985, *Ap. J. Suppl.*, **57**, 621.
Kundu, M. R., Schmahl, E. J., and Velusamy, T. 1982, *Ap. J.*, **253**, 963.
Livshits, M. A., Badalyan, O. G., Kosovichev, A. G., and Katsova, M. M. 1981, *Solar Phys.*, **73**, 269.
MacNeice, P., McWhirter, R. W. P., Spicer, D. S., and Burgess, A. 1984, *Solar Phys.*, **90**, 357.
Mariska, J. T., Emslie, A. G., and Li, P. 1989, *Ap. J.*, **341**, 1067.
McClymont, A. N. 1990, in preparation.
Nagai, F., and Emslie, A. G. 1984, *Ap. J.*, **279**, 896.
Neupert, W. M. 1968, *Ap. J. (Letters)*, **153**, L59.
Orwig, L. E., Frost, K. J., and Dennis, B. R. 1980, *Solar Phys.*, **65**, 25.
Pallavicini, R., Serio, S., and Vaiana, G. S. 1977, *Ap. J.*, **216**, 108.
Pallavicini, R., Peres, G., Serio, S., Vaiana, G., Acton, L., Leibacher, J., and Rosner, R. 1983, *Ap. J.*, **270**, 270.
Simnett, G. M. 1983, *Solar Phys.*, **86**, 289.
Smith, D. F., and Harmony, D. F. 1982, *Ap. J.*, **252**, 800.
Somov, B. V., Sermulina, B. J., and Spektor, A. R. 1982, *Solar Phys.*, **81**, 281.
Somov, B. V., Syrovatskii, S. I., and Spektor, A. R. 1981, *Solar Phys.*, **73**, 145.
Sturrock, P. A. 1973, in *Symposium on High Energy Phemomena in the Sun*, ed. R. Ramaty and R. G. Stone (Goddard SFC Rept. X-693-73-193), p. 3.
Svestka, Z. 1976, *Solar Flares* (Dordrecht: Reidel).

© American Astronomical Society • Provided by the NASA Astrophysics Data System

1990ApJ...348..333C

Tang, F. 1983, *Solar Phys.*, **83**, 15.
Uchida, Y., and Shibata, K. 1988, *Solar Phys.*, **116**, 291.
van Beek, H. F., Hoyng, P., Lafleur, B., and Simmett, G. M. 1980, *Solar Phys.*, **65**, 39.
Winglee, R. M., Pritchett, P. L., and Dulk, G. A. 1988, *Ap. J.*, **329**, 440.
Zarro, D. M., Canfield, R. C., Strong, K. T., and Metcalf, T. R. 1988, *Ap. J.*, **324**, 582 (Paper I).
Zarro, D. M., Slater, G. L., and Freeland, S. L. 1988, *Ap. J.* (*Letters*), **333**, 1199.

RICHARD C. CANFIELD and THOMAS R. METCALF: Institute for Astronomy, University of Hawaii, 2680 Woodlawn Drive Honolulu, HI 96822

JAMES R. LEMEN: Lockheed Palo Alto Research Laboratory, Palo Alto, CA 94304

DOMINIC M. ZARRO: Applied Research Corporation at NASA/Goddard Space Flight Center, Code 602.6, Greenbelt, MD 20771.

© American Astronomical Society • Provided by the NASA Astrophysics Data System